Journal of Applied Fluid Mechanics, Vol. 16, No. 8, pp. 1627-1639, 2023.
Available online at www.jafmonline.net, ISSN 1735-3572, EISSN 1735-3645.
https://doi.org/10.47176/jafm.16.08.1697

Numerical Analysis of the Flow Structure around Inclined Solid Cylinder and Its Effect on Bed Shear Stress Distribution

M. Aksel †

Alanya University, Civil Engineering Department, Alanya, Antalya, Turkey

†*Corresponding Author Email: murat.aksel@alanya.edu.tr*

ABSTRACT

The flow-inclined cylinder interaction is an application area in the industry (i.e., offshore wind turbines and pile-supported near-shore structures). Findings of recent studies have revealed the significance of eco-friendly coastal structures that needs the utilization of inclined cylinder. The primary purpose of this study was to better understand the influence of inclination on flow, turbulence, and bed shear stress character. To achieve this objective, a three-dimensional numerical code (the Reynolds-averaged Navier-Stokes model) was used. The numerical model was calibrated based on eleven velocity profiles obtained by point measurements data of the wake region of the inclined cylinder. The mean flow, turbulence, and secondary flow characteristics around the bodies were extensively investigated, particularly at points where experimental measurements are inapplicable with intrusive turbulence measurement devices. The findings of the study revealed that as the inclination of the cylinder increased, the coherent structures that largely control the flow dynamics in the wake zone became stable rather than cyclical. Specifically, it was determined that although vorticity couples underpinned the flow field behind the vertical cylinder, large-scale streamwise vortices replaced the visible coherent structures when the cylinders were inclined (LSCSVs). When the cylinder inclined 42 degrees, the reduction in amplification factor ($\tau 0$ / $\tau \infty$) over the bed was roughly fifty percent in terms of quantity. This finding shows that inclination is a streamlined form for a cylinder and may reduce the collapse risk due to scour.

Article History

Received December 5, 2022
Revised April 1, 2023
Accepted April 3, 2023
Available online May 31, 2023

Keywords:

Coherent structures
Flow-cylinder interaction
Wake region
Turbulence
Vortices
Helicity
CFD

1. INTRODUCTION

An obstacle exposed to flow receives a drag force due to the interaction between the body and the fluid surrounding it. Because the circular cylinder has extensive applicability in the industry, as a well-defined obstacle compared to others, it has received significant attention in the literature (Norberg, 1994; Sumer & Fredsøe, 2006; Sumner, 2010; Rajani et al., 2012). The typical secondary flow structures, which take place around cylinders are lee-wake vortices, downflow (Yagci et al., 2017), horse-shoe vortices (Unger & Hager, 2006), large-scale counter-rotating streamwise vortices (Roulund et al., 2005a; Baykal et al., 2015), small-scale eddies (Chang & Constantinescu, 2015), and surface roller (Istiarto, 2001; Choi & Choi, 2016; Keshavarzi et al., 2017). The strength and size of these generated coherent flow patterns are considerably controlled by the obstacle geometry, flow, and fluid features.

In recent years, with the increasing utilization of offshore wind turbines, the applicability of tripod-type foundations has enhanced significantly. A tripod-type foundation supporting structure for a wind turbine consists of three inclined cylinders connected by structural elements. Another application field for inclined cylinders is the pile-supported emerged structures (e.g., surface piercing) (Yu, 2002; Acanal et al., 2013; Yagci et al., 2014). These eco-friendly structures do not stop the longshore and cross-shore sediment transport which is vital for sustainable coastal protection projects. Flow-inclined cylinder interaction is also widely seen in natural rivers. The trunky riparian vegetation in natural rivers bends and sways under the influence of the drag force and cyclic motion of vortex shedding (Yagci et al., 2016). Likewise, in coastal waters, mangrove trunks embrace a large number of inclined cylinders (Kazemi, 2017; Wang et al., 2020; Minor et al., 2021).

Surry and Surry (1967) pointed out that energy in the Strouhal peak disperses and diminishes with increasing

Nomenclature

$A_{(x,y,z)}$	directional open area to flow	u'	fluctuation part of the velocity component in streamwise direction
$b_{(x,y,z)}$	directional flow losses	U∞	undisturbed velocity component in streamwise direction
D	cylinder diameter	V	flow velocity
$G_{(x,y,z)}$	directional body forces	V_F	fractional volume open to the flow
$f_{(x,y,z)}$	directional viscous accelerations	v_k	diffusion coefficient of κ_T
H	helicity	α	inclination angle of the cylinder
P	pressure	γ	specific gravity of the fluid
R	coordinate system-controlled flow coefficient	ε_T	turbulence dissipation
R_{DIF}	turbulent diffusion	ξ	coordinate conversion coefficient
R_{SOR}	mass source	κ_T	turbulence kinetic energy (TKE)
t	time domain	ρ	density of the fluid
$<u>$	depth-averaged mean of velocity component in streamwise direction	τ_0	bed shear stress
u	velocity component in streamwise direction	τ_∞	undisturbed bed shear stress
$\bar{u}$	time-averaged mean of velocity component in streamwise direction	ω	vorticity

inclination. Recent studies have shown that the inclination of a cylinder affects the generated flow field dramatically. Kitsikoudis et al. (2017) demonstrated that due to the inclination, the strength of downflow decreased and the flow recovered at a shorter distance near the bed region compared to the upright counterpart (Kitsikoudis et al., 2017). According to Graf and Istiarto (2002), the strength of horse-shoe vortices largely depends on the strength of the downflow. From this point of view, the inclination of a cylinder against the flow can be considered as the transformation of the cylinder into a more streamlined form as previously stated by Majd et al. (2016). According to Majd et al. (2016), this streamlining due to inclination makes the pile's cross-sectional area elliptical and suppresses the vortex production process. Furthermore, the flume experiments by Majd et al. (2016) revealed that the inclination significantly changed the cylinder's upstream separation distance and affected the strength of the horse-shoe vortices, possibly resulting from this separation. Shang et. al. (2018) investigated the influence of the cylinder's curvature on the flow field. Their findings pointed out that the flow separation and reattachment points shifted downstream with the increase in curvature of the cylinder. The critical curvature, which controls the existing flow character, can be defined as the reattachment point where it coincides with the separation point. The wake behind a quarter-of-ring concave curved cylinder is highly steady on low Reynolds numbers (Re⩽300). At Re 400 and 500, the changes are continuous which results in a frequency band in the 3D energy spectrum via direct numerical solution (Jiang et al., 2018). Jiang et al. (2019) showed that large-scale and unstable vortices are generated in the wake of a concave-curved cylinder. These three-dimensional asymmetric vortices exhibit very unstable character. In a broad sense, this observed flow instability is greatly dependent on/or Reynolds and Froude numbers depending on the flow features. Additionally, Chiatto et. al. (2021) examined the effect of the cylinder's curvature on flow separation, reattachment points and pressure drag, and they identified critical values at which the flow became unsteady, and the drag coefficient increased. This flow structure altering due to the inclination of the cylinder has certain reflections in terms of morphological adjustments (i.e., scour process) on the bed of riverine and coastal domains. As the inclination increases, the local scour depth around a bridge pier is diminished considerably (Bozkus & Yildiz, 2004; Euler et al., 2014; Kitsikoudis et al., 2017). All these findings make the inclined cylinder an appropriate option as a supporting structure that can be employed in offshore turbines and surface-piercing coastal structures (e.g., inclined thin plates and wave screens).

Although a significant background regarding the flow-inclined cylinder interactions is available in the pertinent literature, there is still a lack of knowledge regarding the hydrodynamic perspective of the problem. More specifically, while the previous studies have mainly focused on the problem within the kinematic perspective and aimed to resolve the coherent flow structures generated around the inclined cylinder (e.g., downflow, lee-wake vortices, or horseshoe vortices) based on point measurements, the following research questions have remained unanswered.

1) How does the inclination angle control the spatial distribution of shear stress on the surface of the cylinder and near the bottom around the body?

2) Depending on the inclination how does the flow field change immediately downstream of inclined cylinders, which could not be measured in previous studies with existing ADV technologies?

3) How does the bed shear stress change depending on the inclination of a cylinder?

The primary objective of this study is to answer the following research questions on a quantitative base. While doing both spatial and temporal analyses were conducted and the obtained results were presented in both Eulerian and Lagrangian manner.

2. METHODOLOGY

In order to achieve the described objective above, a quantitative study was carried out. In a typical flume or field experiment, the flow fields are determined based on point measurements. However, it is not practically possible to detect all the flow domain since the probe of the Acoustic Doppler Velocimeter (ADV) is bulky. Besides, it is impractical to measure certain physical variables in a flume experiment. For instance, the shear stress distribution around/on the surface of the obstacle or measuring the pressure distribution over the surface of the inclined cylinder is not practically easy and requires the utilization of intrusive instruments. The use of intrusive instruments (i.e., pressure transducer or hot-film anemometer) may disturb the flow field and may affect the obtained results. Because of this, numerical models emerge as efficient and cost-effective tools. Such an approximation allows examining the flow field in a more detailed manner if the model is calibrated well based on a reliable experimental dataset.

Within this context, a Reynold-Averaged Navier-Stokes (RANS) model was run in this study. The experimental data generated by Kitsikoudis et al. (2017) constituted the core of the numerical model. The identical flow conditions were created in the numerical flow domain and the inclination angles of α = 0°, 14°, and 42° were examined. The comparison between experimental and numerical outputs was carried out regarding the experimental measurement grid applied by Kitsikouidis et al. (2017). The description of the numerical model and the validation dataset ss given below.

The given numerical analysis was carried out based on a dataset generated from a flume experiment. Water depth, discharge, and channel bottom slope were held constant throughout the numerical research in accordance with this dataset. As a result, the influence of these three variables was omitted, and the simulations focused solely on the role of cylinder inclination on the flow structure in the wake region.

2.1 Basic Definitions Used in the Analysis

In turbulent flow, the velocity component for streamwise direction can be defined as in Eq. 1.

$$u = \bar{u} + u' \tag{1}$$

where, u is the velocity component for streamwise direction, $\bar{u}$ is time-averaged mean velocity value and u' is the fluctuation part. The Reynolds decomposition is another name for this representation (Rosa, 2006; Nieuwstadt et al., 2016).

It is well-known that clear-water free surface flow mostly has a higher Reynolds number, and the regime is turbulent. Turbulence kinetic energy (TKE) is the key parameter to characterize turbulence in a flow domain. To calculate TKE one-equation-based turbulence models use root-mean-square (RMS) means of turbulence fluctuation components and for a three-dimensional flow this can be shown as follows:

$$\kappa_T = \frac{1}{2}\left(\overline{u'^2} + \overline{v'^2} + \overline{w'^2}\right) \tag{2}$$

In Eq. 2, u', v', and w' are the directional chaotic turbulent fluctuations for x, y, and z in cartesian coordinates, respectively (Flowscience, 2019).

In fluid dynamics literature vorticity is the main actor to depict to present vortices. Vorticity can be defined simply as twice the angular velocity vector of the rotation. The quantity of "circulation" or "rotation" (or, more precisely, the local angular rate of rotation) in a fluid can be associated with vorticity. In cartesian coordinates, vorticity is

$$\omega = \nabla x\ V \tag{3}$$

Under certain conditions, with a topological interpretation as a measure of the connection and/or knottedness of vortex lines, helicity is an invariant of the Euler equations of fluid flow (Moreau, 1961; Moffatt, 1969). It is a kind of way to visualize vortex cores inside a turbulent flow domain and can be defined as a starting point to investigate the fluid flow turbulence (Zimmerman, 1996).

Helicity can be expressed by the formula given in Eq. 4.

$$H = \int_V u\ .(\nabla\ x\ u)\ dV \tag{4}$$

where "H" refers to the scalar helicity magnitude inside a flow domain which can be calculated using the u (x, t) velocity field and ω (x, t), vorticity field (Moffatt, 1969). The density of the helicity depending on temporal and spatial conditions can be defined as follows:

$$h(x,t)\ =\ u\ x\ \omega \tag{5}$$

Both helicity (H) and the density of the helicity (h) are pseudoscalar quantities, and their symmetry is equivalent to the reflection in a plane (i.e., space inversion or parity transformation). Helicity is vital in flow kinematics since it allows for topological interpretation concerning the connection or linkages of flow vortex lines (Moffatt & Tsinober, 1992). In their study, Moffat and Tsinober (1992) pointed out the relationship between helicity and vortex breakdown. Helicity and helicity density are used to characterize helical coherent structures in turbulence and cause in significant results with direct practical engineering (Yamamoto & Hosokawa, 1981; Tesař, 2005).

2.2 Description of the Hydrodynamic Model

Governing equations

Incompressible RANS equations are solved using the finite volume approximation in Flow 3D. Several hydraulic and coastal engineering applications have been carried out with this model in previous research. The most general form of the three-dimensional versions of the used governing equations (for the incompressible fluid case) is shown below.

Mass continuity

$$V_F \frac{\partial \rho}{\partial t} + \frac{\partial}{\partial x}(\rho u A_x) + R\frac{\partial}{\partial y}(\rho v A_y) + \frac{\partial}{\partial z}(\rho w A_z) + \xi \frac{\rho u A_x}{x} = R_{DIF} + R_{SOR} \tag{6}$$

In Eq. 6, V_F denotes the fractional volume open to the flow and the coefficient R is controlled by the coordinate system chosen in the following way. R_{DIF} and R_{SOR} terms, given on the right side of Eq. 6 symbolize diffusion turbulent and mass source, respectively. These terms are given in the following equations:

$$R_{DIF} = \frac{\partial}{\partial x}\left(\nu_p A_x \frac{\partial \rho}{\partial x}\right) + R\frac{\partial}{\partial y}\left(\nu_p A_y \frac{\partial \rho}{\partial y}\right) + \frac{\partial}{\partial z}\left(\nu_p A_z \frac{\partial \rho}{\partial z}\right) + \xi\frac{\rho \nu_p A_x}{x} \quad (7)$$

$$R_{SOR} = \rho\left(\frac{V_F}{\rho c'}\frac{\partial P}{\partial t} + \frac{\partial u A_x}{\partial x} + R\frac{\partial v A_y}{\partial y} + \frac{\partial w A_z}{\partial z} + \xi\frac{u A_x}{x}\right) \quad (8)$$

Momentum

Momentum transfers in the flow domain for three dimensions are given in Eq. 9.

$$\begin{aligned}
&\frac{\partial u}{\partial t} + \frac{1}{V_F}\left\{uA_x\frac{\partial u}{\partial x} + vA_y\frac{\partial u}{\partial y} + wA_z\frac{\partial u}{\partial z}\right\} - \zeta\frac{A_y v^2}{xV_F} = \\
&-\frac{1}{\rho}\frac{\partial P}{\partial x} + G_x + f_x - b_x - \frac{R_{SOR}}{\rho V_F}(u - u_w - \delta u_s) \\
&\frac{\partial v}{\partial t} + \frac{1}{V_F}\left\{uA_x\frac{\partial v}{\partial x} + vA_y\frac{\partial v}{\partial y} + wA_z\frac{\partial v}{\partial z}\right\} + \zeta\frac{A_y uv}{xV_F} = \\
&-\frac{1}{\rho}\frac{\partial P}{\partial y}R + G_y + f_y - b_y - \frac{R_{SOR}}{\rho V_F}(v - v_w - \delta v_s) \\
&\frac{\partial w}{\partial t} + \frac{1}{V_F}\left\{uA_x\frac{\partial w}{\partial x} + vA_y\frac{\partial w}{\partial y} + wA_z\frac{\partial w}{\partial z}\right\} = -\frac{1}{\rho}\frac{\partial P}{\partial z} + G_z + \\
&f_z - b_z - \frac{R_{SOR}}{\rho V_F}(w - w_w - \delta w_s)
\end{aligned} \quad (9)$$

where $G_{(x,y,z)}$ are body force components, $A_{(x,y,z)}$ are the directional open area to flow, f is viscous force, b is flow losses in porous media/across porous baffle plates, and the final terms account for the injection of mass at a source represented by a geometry component (Flowscience, 2019).

Turbulence closure

The transport equation for turbulent kinetic energy (k_T) incorporates turbulent kinetic energy convection and diffusion, turbulent kinetic energy generation due to shearing and buoyancy effects, diffusion, and dissipation due to viscous losses within turbulent-caused eddies (Flowscience, 2019). The formula of two turbulence model equations (i.e., k – ε and k – ω) for the k_T and their dissipation depending on ε_T and ω are given below, respectively.

$$\frac{\partial k_T}{\partial t} + \frac{1}{V_F}\left\{uA_x\frac{\partial k_T}{\partial x} + vA_y\frac{\partial k_T}{\partial y} + wA_z\frac{\partial k_T}{\partial z}\right\} = P_T + G_T + Diff_{kT} - \epsilon_T \quad (10)$$

$$\frac{\partial k_T}{\partial t} + \frac{1}{V_F}\left\{uA_x\frac{\partial k_T}{\partial x} + vA_y\frac{\partial k_T}{\partial y} + wA_z\frac{\partial k_T}{\partial z}\right\} = P_T + G_T + Diff_{kT} - \beta^* k\omega \quad (11)$$

In these turbulent transport equations (Eq. 10 & 11), P_T, G_T and $Diff_{kT}$ are transport equations for the turbulent kinetic energy, the buoyancy production, and the diffusion term, respectively (Flowscience, 2019).

2.3 Model Specifications

Initial and Boundary Conditions

The numerical model was prepared based on the experimental study of Kitsikouidis et al. (2017). The model domain was defined as the same volume as the flume used in the experiments. As an initial water level in the flow domain, the depth of the water was taken as 0.3 m. The volume of fluid (VOF) method was selected to define the two-phase (air-water) open channel flow condition. Side walls and the bottom of the flume were selected as wall boundary conditions with no-slip. The upward boundary condition was chosen as a pressure-type boundary condition and specified as zero relative pressure. The velocity of water at the inlet boundary was specified as 0.214 m/s with a constant depth (i.e., 0.3 m), which is near a cylinder Reynolds number of 35000. A constant water depth, which was the same as the initial or inlet depth and enabled water to leave the flow domain, was defined in the outlet boundary.

Discretization of the Flow Domain

A quadratic type of mesh was applied to the flow domain with a refinement zone that encapsulated the cylinder bodies. The computational flow domain, which replicates the flume dimensions with 60D, 10D, and 5D in the x, y, and z directions, respectively, is presented in Fig. 1. The mesh quality around the cylinder was improved using three-nested mesh blocks to keep the cylinder form. The flow domain and the mesh characteristics for nesting zones are shown in Fig. 1. From the outer zone to the inner nesting zone, the mesh size was specified as 0.22D, 0.11D, and 0.055D, gradually. That is, throughout the nesting process, the growth rate was maintained at 2 times.

2.4 Validation/Calibration of the Numerical Model

The efficiency of two different turbulence models, k-ω and standard k-epsilon were tested for the representation of turbulence behavior with an acceptable accuracy around /behind the pile. The numerical trials showed that the k-ω turbulence model slightly better fit with the data compared to the k-epsilon model (Fig. 2). The high efficiency of the k-ω closure model in the case of boundary-layer flows with a strong adverse pressure gradient or flow separation has already been shown in the related literature (Roulund et al., 2005b; Baykal et al., 2015; Larsen et al., 2016) Based on this result, k-ω turbulence closure was utilized throughout the numerical study.

Once the turbulence closure (i.e., k-ω turbulence model) was selected, the sensitivity of the obtained results to certain model variables was tested by a series of numerical trials. In these trials, the roles of surface roughness of the flume and pile, and the fluid viscosity were tested. The role of surface roughness on the obtained depth-averaged streamwise velocity, $(\langle\bar{u}\rangle)/U_\infty$ is shown in Fig. 2a. To make a comparative analysis between the imposed surface roughness values in the model, the results were presented together with experimental data in Fig. 2b. The applied tests showed that Scenario 2 was the most convenient surface roughness for the model in terms of representation of the surface with acceptable accuracy. Furthermore, the influence of viscosity was also tested during the preliminary numerical tests. While deciding about the candidate dynamic viscosity values for the viscosity of the water, probable values which may exist during the indoor experiments were chosen. As can be in Fig. 2c, these values correspond to the viscosity of water

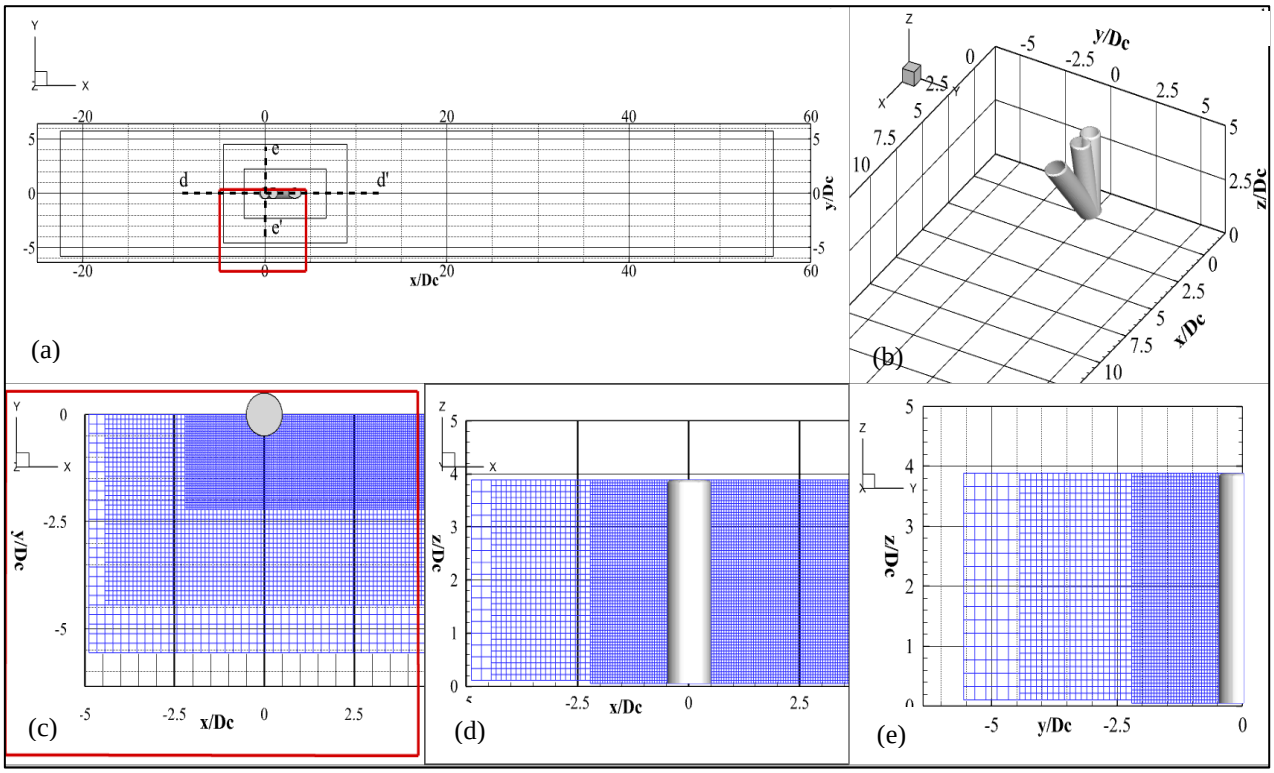

Fig. 1. Basic characteristics of a) flow domain with cylinders b) isometric view of the examined cylinders (i.e., 0° (upright), 14°, and 42°), nesting mesh zones with blue colored elements c) plan view d) side view, and e) front view.

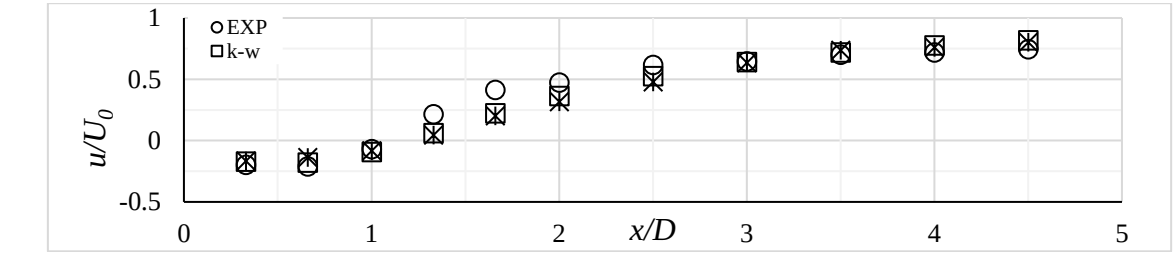

(a)

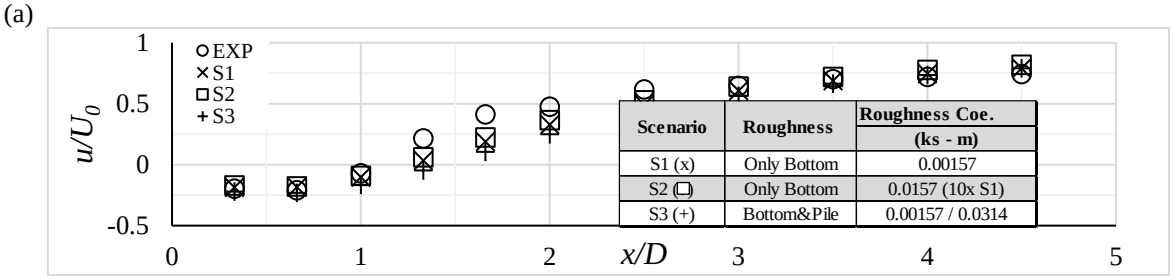

Scenario	Roughness	Roughness Coe. (ks - m)
S1 (x)	Only Bottom	0.00157
S2 (□)	Only Bottom	0.0157 (10x S1)
S3 (+)	Bottom&Pile	0.00157 / 0.0314

(b)

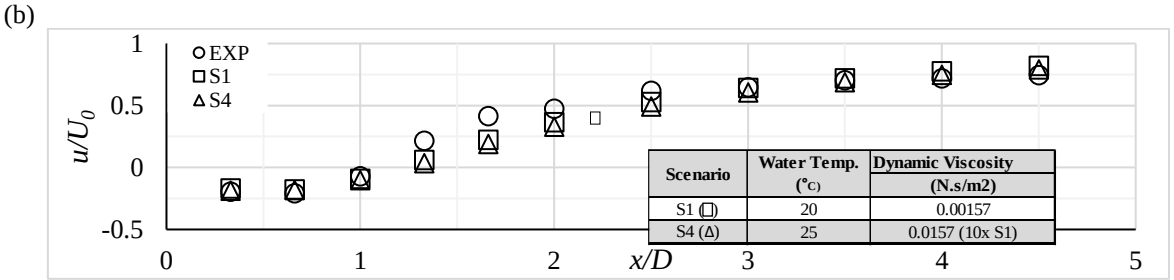

Scenario	Water Temp. (°C)	Dynamic Viscosity (N.s/m2)
S1 (□)	20	0.00157
S4 (Δ)	25	0.0157 (10x S1)

(c)

Fig. 2. The progression of depth-averaged velocity, $< \bar{u} > / U_{\infty}$, in streamwise direction: Comparison of the experimental measurements with numerical outputs for different a) turbulence models b) roughness coefficients, and c) dynamic viscosity values of water.

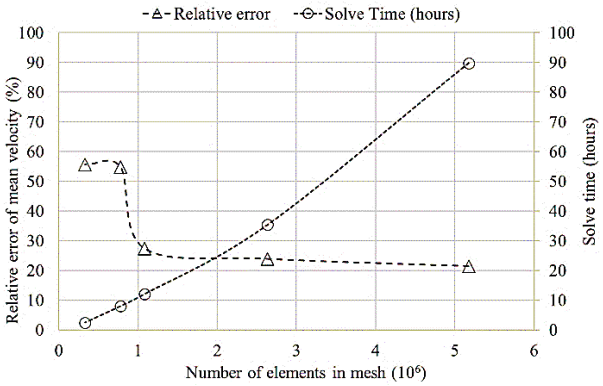

Fig. 3. Model convergence analysis due to number of mesh elements.

at 20 °C and 25 °C. The numerical trial revealed that the viscosity value of water corresponding to 20 °C fits better with experimental values. To be able to make comparison, the computational domain of the study was the same as the experimental setup used in Kitsikouidis et al. (2017).

When the model's performance shown in Fig. 2 is examined, (except for the distances 1.25(X/D) and 2.5(X/D)), it was determined that the model outputs were in perfect agreement with the experimental dataset. However, in the spatial interval between 1.25(X/D) and 2.5(X/D), the model outputs exhibited a little deviation from the experimental data. This interval is related to the region where the interaction of the vortices largely controls the mixing process in the wake region.

In the graph given in Fig. 3, the horizontal axis represents the number of elements, the primary vertical axis (left) represents the relative error percentage of the depth-averaged velocity based on experimental results at calculation points, and the right axis represents the model calculation time. Based on these model conditions, it can be said that the model converges at an acceptable accuracy level starting from the $2x10^6$ element numbers.

3.ANALYSIS OF THE RESULTS

As mentioned in the introduction section, the major goal of the study was to determine the role of the inclination angle on the resultant hydrodynamic loads acting on the cylinder. Therefore, during the presentation of the results, firstly, the flow kinematic around the body was analyzed, since it was considered that it might facilitate understanding the dynamic analysis.

3.1 Flow Kinematics – Time Averaged Analysis

In Fig. 4, the spatial variations of the time-averaged streamwise velocity in the wake region are given for different inclination angles. As can be seen in Fig. 3a1, due to bed-generated turbulence, flow recovers near the bed earlier when the cylinder is upright. This finding is consistent with Kitsikoudis et al. (2016). With the inclination of the cylinder due to mitigated downflow strength (Fig.4-1) and diminished turbulence (TKE chart) near the bed rear of the cylinder (Fig. 4-2), the flow domain in the wake region changes dramatically. The quick recovery zone which was observed near the bed for the upright cylinder in Fig. 4a1 vanished for two inclined cylinder cases as seen in Fig. 4b1 and 4c1.

In other words, it was determined that for the inclined cases, the flow recovery process was delayed in the wake region near the bed. Consequently, for these cases, prominent negative streamwise velocities (i.e., recirculation zone) were observed near the bed in the wake region. It is also seen in Fig. 5 that this situation becomes more evident with the enhanced inclination angle. In summary, with the inclination effect the downflow weakens, the pile's cross-sectional area gets elliptical, and this streamlined cross-section significantly suppresses the vortex-induced turbulence generation. Presumably, because of the enhanced recirculation zone observed near the bed for inclined cases (Fig. 5b1 and 5c1), downstream of the scour holes the eroded bed has a less steep surface as can be seen from Figures 4b-4d and Fig. 5 in Kitsikouidis et al. (2017). However, except bed region rear of the obstacle, the vertical velocity components, except bed region rear of the obstacle, decline with the inclination angles of the cylinder.

When the TKE values behind the cylinders (Fig. 6b2 and 5b3) are comparatively analyzed it can be concluded that even a small inclination angle causes a significant drop in turbulence. This outcome is also related to the fact that due to the inclination of the cylinder the pile's cross-sectional area gets elliptical and this situation suppresses the generation pairs of vortices. It is a well-known fact that the elliptical cross-sectional form is a better hydrodynamic form compared to the cylindrical one (Munson et al., 2002). Another consequence that can be inferred from Fig. 6 is that with the increasing inclination angle, the streamwise velocity at the upstream centerline of the flume increases (Fig. 6a1-c1). This can be considered clear evidence that with the inclination of the cylinder, the backwater effect decreases due to decreased hydrodynamic resistance. In addition, it was observed that TKEs were higher near the bed, upstream of the inclined cylinders for inclined cases compared to that of the upright cylinder. These findings are consistent with Sumer and Fredsøe (2006) who stated that the direction of velocity passing around the cylinder is perpendicular pile axis.

As seen in Fig 5, negative vertical time-averaged velocity values were observed in front of the upright cylinder. With the increasing inclination angle, those negative vertical velocity values in front of the cylinder changed to positive values. Positive values imply that the vertical component of the water-mass transport towards the water surface. Based on this, it can be concluded that the decrease in downflow can be seen as one of the major consequences of inclined cylinders being more streamlined forms. When the vertical velocities just around the surface of the cylinders are examined in Fig. 5, it can be inferred that the vertical component of the resultant flow vectors increases with the increasing

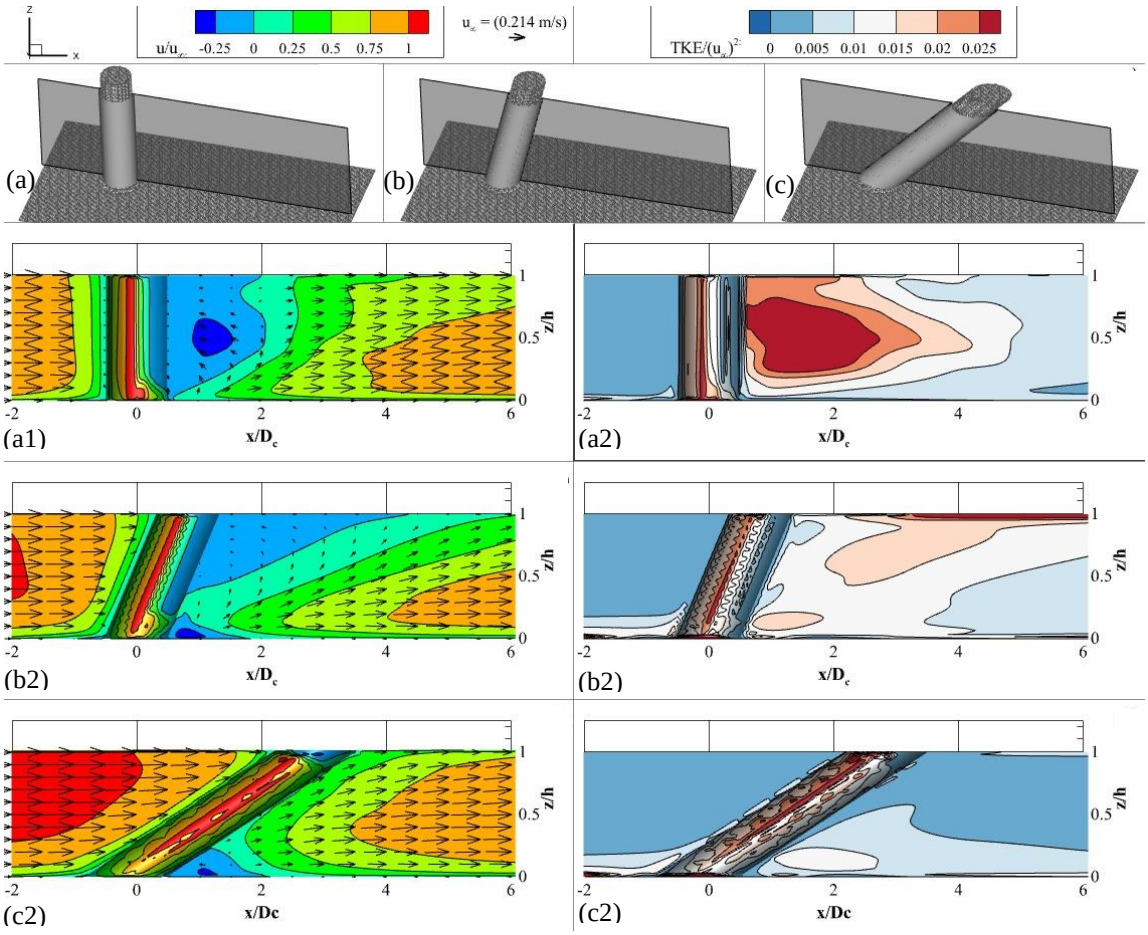

Fig. 4. The spatial variation of time-averaged streamwise velocity and turbulence kinetic energy at the centerline of the flume and side-surface of the cylinder for the cases a) upright cylinder (i.e., 0°), b) 14°, c) 42°. The indices of 1 and 2 indicate streamwise velocity and TKE, respectively for the relevant case.

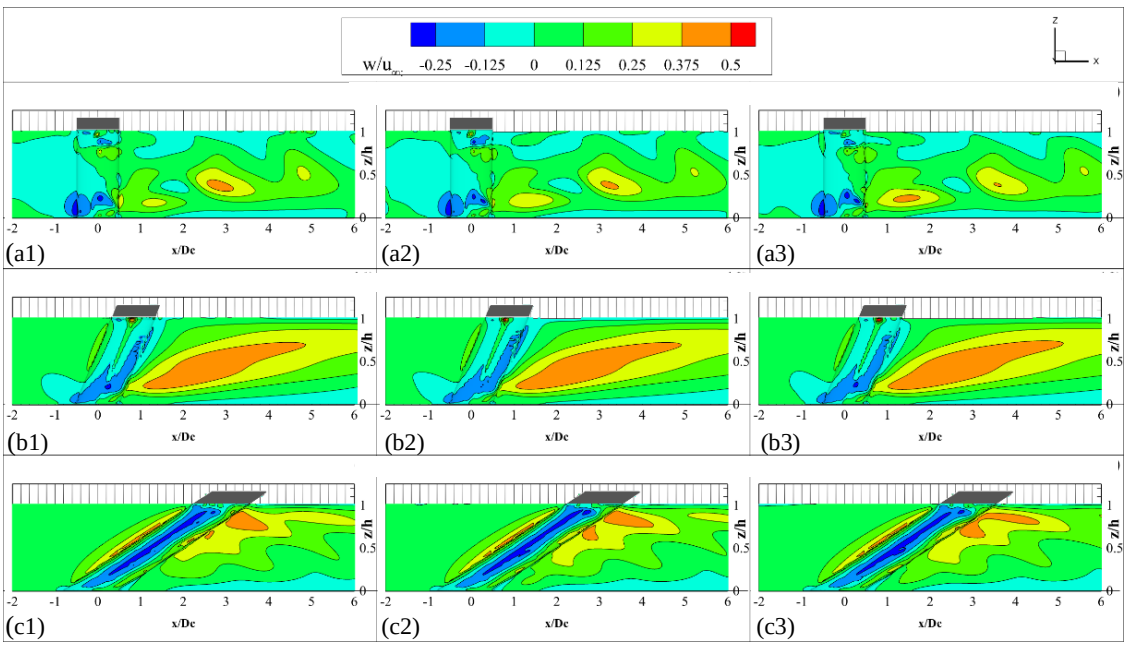

Fig. 5. Instantaneous normalized vertical velocity patterns for three consecutive moments at the centerline of the flume and side-surface of the cylinder. The time-intervals between the frames were selected as one-third of the vortex shedding frequency.

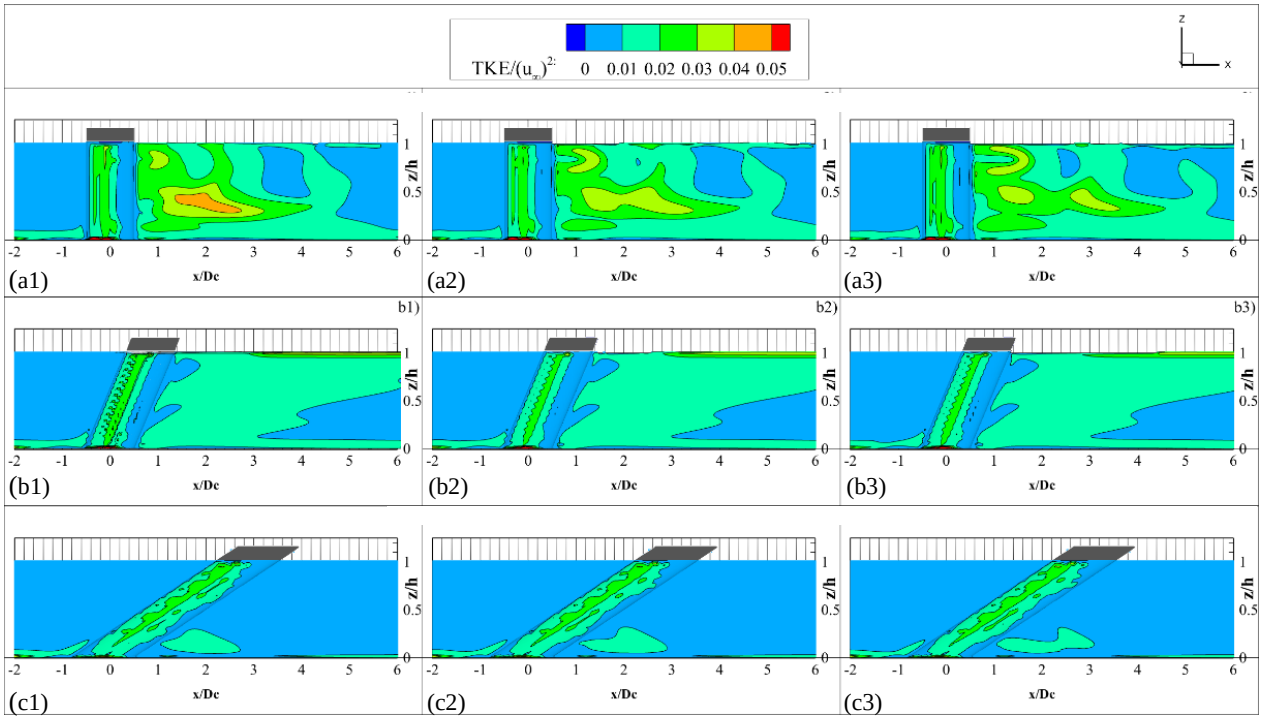

Fig. 6. Instantaneous normalized turbulent kinetic energy for three consecutive moments at the centerline of the flume and side-surface of the cylinder. The time-intervals between the frames were selected as one-third of the vortex shedding frequency.

inclination angle of the cylinder. However, it is also worth highlighting that this increment in vertical velocity does not exhibit a monotonic pattern with inclination.

The downflow, which is pointed out as the source of coherent structures in the wake region by Unger and Hager (2006) is examined in Fig. 4. The time intervals between the moments in Fig. 5 are one-third of the vortex shedding frequency. It is seen in Fig. 5 that while the vertical velocity patterns behind the upright cylinder exhibit a noticeable variability over time, this variability in the spatial vertical velocity patterns entirely disappears for inclined cases. These time-independent spatial patterns suggest that the coherent structures, which control the flow dynamics in the wake region, exhibit a steady character (i.e., time-independent) rather than having a cyclic character. The temporal variations (i.e., three consecutive sequence) of turbulence kinetic energy (TKE) patterns observed given in Fig. 6b also confirms this steady character of flow in the wake region. Figure 6 also confirms how inclination in the cylinder suppresses the turbulence production.

3.2 Kinematic Analysis-instantaneous Coherent Flow Patterns

It is clear that the alteration in obstacle geometry brings about the boundary layer development and the flow pattern in the wake region. From this perspective, the effect of the inclination of the isolated cylinder on the flow structures behind the cylinders was also investigated. The figure shows instantaneous streamlines for the three analyzed cylinder instances. As seen in Fig. 7, the large-scale counter-rotating streamwise vortices replace the prominent coherent structures with the inclination of the cylinders, while the vorticity pairs suppress the flow field near the obstruction for the upright case cylinder (LSCSVs).

As emphasized above, the inclination controls the pressure distribution around the obstacle and the generation of coherent structures. Figure 7 shows that the LSCSVs get more intense as the inclination angle increases. The pairs of vortices entirely vanish at the 42° angle of the cylinders. From a mechanical standpoint, this condition suggests that boundary layer separation-induced vortices control the flow field and create lee-wake vortices in the upright cylinder at the back of the body. Yet, the pile's cross-section gets more hydrodynamic with inclination; thus, this hydrodynamic cross-section shape prevents the creation of pronounced vortices in the wake zone of the inclined cylinder. As seen in Fig. 7 (streamlines), LSCSVs are particularly well-defined at the 42° angle of the cylinders.

To examine the difference between the character of coherent flow patterns observed around upright and inclined casers more closely, the variation helicity patterns are presented in Fig. 8. These patterns define the isolated vortex cores calculated rear examined obstacles in isometric view. In the subplots shown in Fig. 8, the variations of helicity values are also given for three different cross-sections. Figure 8 clearly shows that the scales of the generated isolated coherent flow structures are dramatically different from each other for upright and inclined cylinder cases. More specifically, behind the case of the upright cylinder the generated isolated flow structures develop distinctively and locally around an

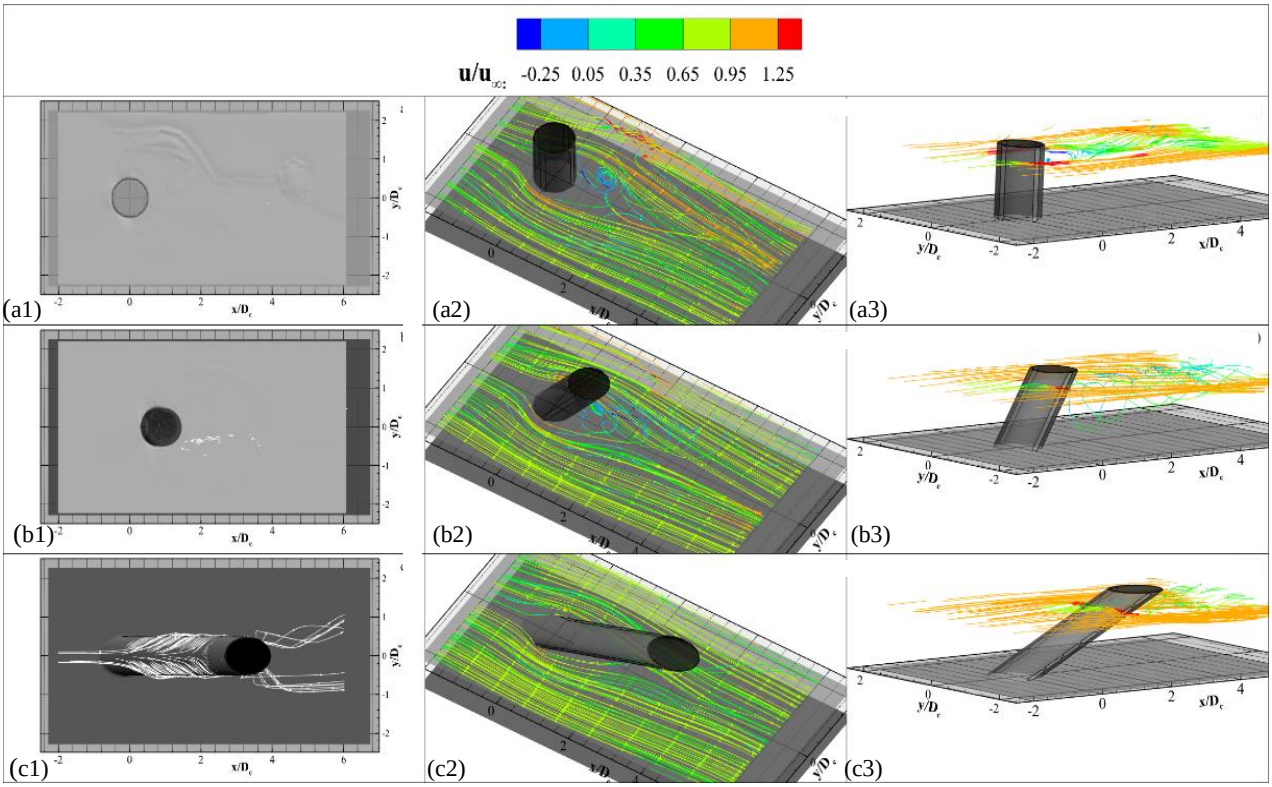

Fig. 7. The influence of inclination on instantaneous streamlines at a) for upright case, b) 14°, c) 42°. The indices of "1" show the streamlines which contact with cylinder surfaces, "2" indicates the streamlines near the bed, and "3" denotes streamlines near the water surface.

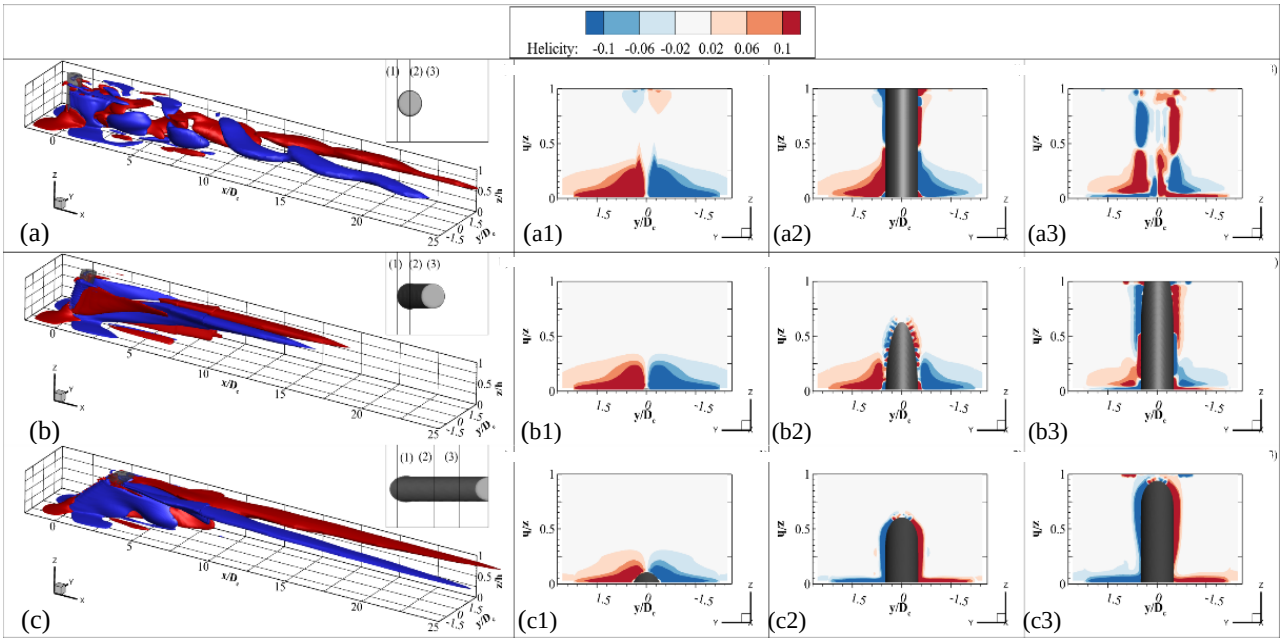

Fig. 8. The helicity patterns as an indicator of prominent secondary flow patterns that occur in the wake region of the different inclination angles of the cylinders.

imaginary axis, while for the inclined cases these secondary flow structures take an elongated form and occupy a relatively larger zone. It can also be deduced that behind the upright cylinder the vortices develop and decay quickly, while in inclined cases the produced pair of vortices stay alive in a relatively larger zone. It is reasonable to suggest that this variation in helicity patterns originates from the difference in shear layer patterns occurring behind the obstructions. When considered from this point of view, it can be said that if the shear layer

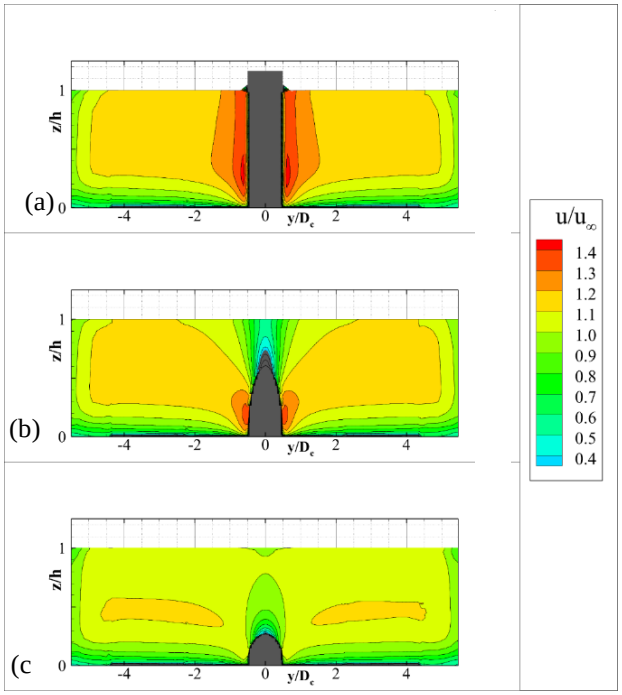

Fig. 9. The influence of the inclination of the cylinders on the contraction effect

greatly controls the flow structure in the wake region, the flow structure emerges as an inevitable consequence of obstacle characteristics. It is expected if the contraction effect is more pronounced, the shear layer's strength will be more noticeable in the wake zone of an obstruction. To show this condition in further detail, the contraction effects of the investigated piles are presented in Fig. 9. As seen in Fig. 9, in the case of the upright cylinder the contraction effect is much stronger than that of inclined counterparts. This means that the velocity deficit between the wake region and contraction region is more pronounced for the upright form of the cylinder.

After the analysis presented above, it was also aimed to investigate other coherent patterns more thoroughly.

3.3 Influence of Inclination on Bed Erodibility

When the flow encounters a bottom-mounted cylinder, the shear stress markedly amplifies around the cylinder (Fig. 10). As a natural consequence of this amplification in shear stress, the bed material becomes vulnerable to being mobilized. Such particle entrainment resulted in scouring around the supporting piles (Ettema et al., 1998; Yagci et al., 2016). Based on this, it can be said that it is reasonable to check the spatial distribution of the time-averaged amplification factor (τ_0/τ_∞) (Fig. 10). Figure 10 clearly points out the influence of inclination on the amplification factor. As seen in Fig. 10, the inclination of the cylinder greatly diminishes the cylinder induced amplification in bed shear stress. Not only the value of the amplification factor decreases around the side-edges of the body, but also the high shear stress zone around the body dramatically decreases on the bed. Quantitatively, this drop in amplification factor over the bed is around 50 %. This result reveals that inclination is a streamlined form for a cylinder and has a great potential for the risk of failure in coastal structures that may arise due to scour.

4. CONCLUSION

In this study, the influence of the inclination of isolated emergent cylinders exposed to flow was numerically investigated. In the scope of the study, three angles (i.e., 0° (upright), 14°, and 42°) were examined. Based on the analysis of the numerical outputs the following findings were attained.

- The analysis reveals that although the vertical velocity characteristics behind the upright cylinder exhibit substantial variation over time, this variability in spatial velocity profiles completely vanishes for inclined situations. These spatial-temporal patterns do not change over time, which suggests that the coherent structures that control the flow dynamics in the wake area are stable rather than cyclical. This means that for the situation of a vertical cylinder, vorticity pairs suppress the flow field behind the obstruction. Nevertheless, when the cylinders are inclined, the obvious coherent structures are replaced by large-scale streamwise vortices (LSCSVs). It is clear that the greater the inclination angle, the more intense the LSCSVs. At a cylinder angle of 42°, pairs of vortices disappear completely. From a mechanical standpoint, this suggests that the boundary layer separation-induced vortices govern the flow field and create lee-wake vortices in the case of the upright cylinder, and rear body. With increasing inclination, however, the cross-section of the pile becomes more hydrodynamic; hence, this hydrodynamic cross-section shape prevents the production of pronounced vortices in the wake zone of the inclined cylinder. LSCSVs are especially well-defined at the cylinder angle of 14°.

In the wake zone of a vertical cylinder, the generated vortices arise distinctively and locally. Yet, in inclined circumstances, these vortices have an elongated form and occupy a significantly greater region compared to the upright case. Also, the vortices in the wake region of the upright cylinder form vividly but fade rapidly in the streamwise direction. On the other hand, the weaker vortices produced behind the inclined cylinders remain energetic in a much broader zone.

- With the inclination of the cylinder, the flow domain in the wake area changes drastically due to the reduced downflow intensity and the pile's cross-sectional area gets elliptical. This streamlined cross-section significantly suppresses the vortex-induced turbulence generation. More explicitly, even a small inclination angle causes a significant decrease in turbulence kinetic energy in the wake zone.

- The swift recovery zone, which is typically observed near the bed for the upright cylinder, entirely disappeared for the two analyzed examples of inclined cylinders. Instead, the concentrated deceleration zone near

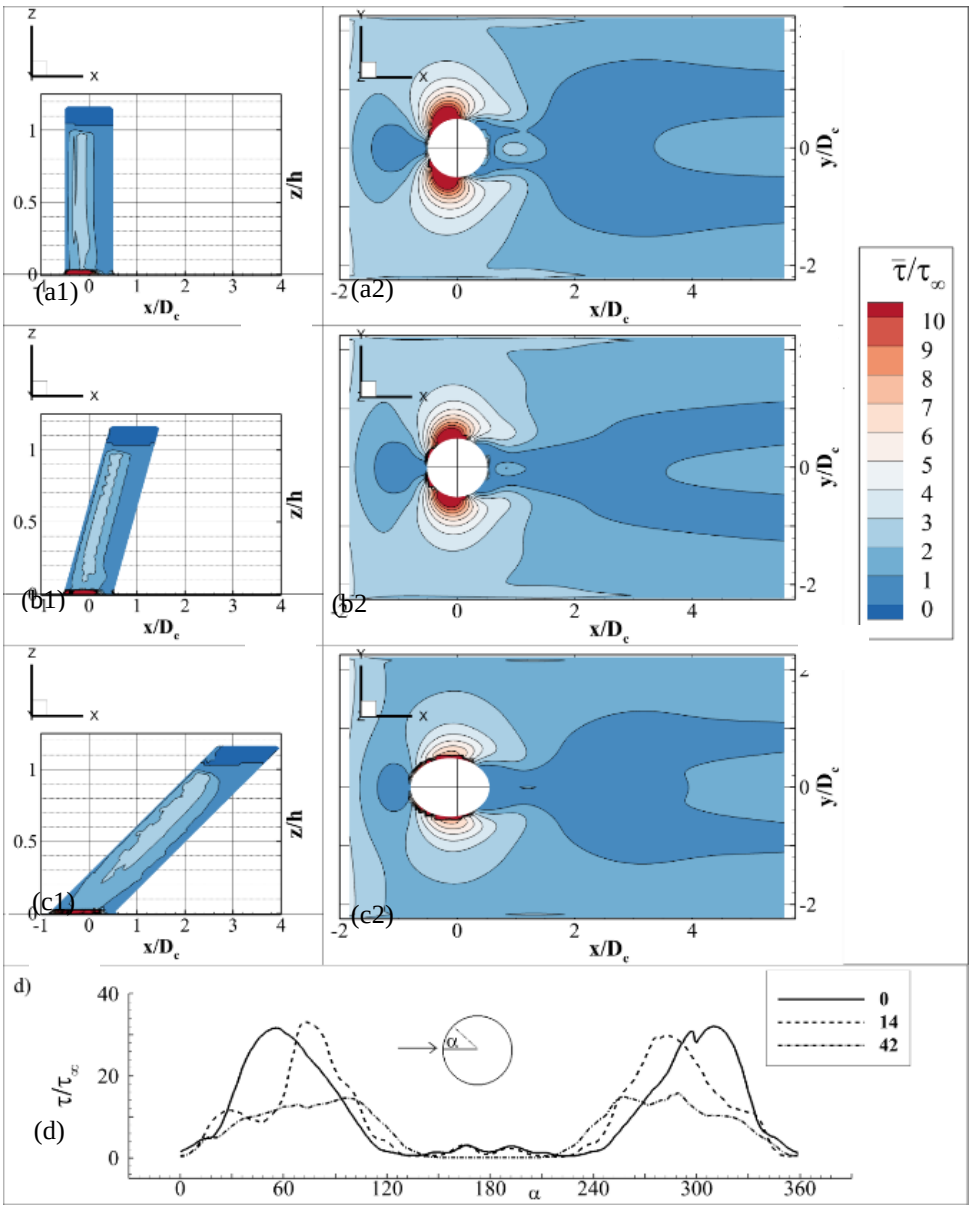

Fig. 10. The variation of amplification factor τ_0/τ_∞ over the surface of bed depending on the inclination of the cylinders.

the bed was observed in the wake region. Presumably because of the enhanced recirculation zone observed near the bed for inclined cases downstream, the scour holes observed in the literature have a less steep surface downstream. It was observed that the vertical components of the resultant flow vectors increased as the inclination angle of the cylinder increased.

• Figure 10 demonstrates that the tilt of the cylinder significantly reduces the amplification of the bed shear stress caused by the cylinder. Not only the amplification factor value drops drastically near the body's margins, but the high shear stress zone on the bed also shrinks significantly. The quantitative loss in bed amplification factor is around half. This finding indicates that an inclination is a more aerodynamic shape for a cylinder, which may significantly reduce the danger of collapse in coastal constructions caused by scour.

ACKNOWLEDGEMENTS

The author would like to thank Kitsikoudis, V., Kirca, V. S. O., Yagci, O., Celik, M. F. for sharing their high precise experimental measurement data.

CONFLICT OF INTEREST

The author declares that he has no known competing financial interests or non-financial interest that could have appeared to influence the work reported in this paper.

AUTHORS CONTRIBUTION

M. Aksel designed the computational framework, carried out the implementation and performed the calculations. M. Aksel post-processed the results and wrote the manuscript.

REFERENCES

Acanal, L., Loukogeorgaki, E., Yagci, O., Kirca, V. S. O., & Akgul, A. (2013). Performance of an inclined thin plate in wave attenuation. *Journal of Coastal Research*, 65 (10065), 141–146 https://doi.org/10.2112/SI65-025.1

Baykal, C., Sumer, B. M., Fuhrman, D. R., Jacobsen, N. G., & Fredsøe, J. (2015). Numerical investigation of flow and scour around a vertical circular cylinder. *Philosophical Transactions of the Royal Society A: Mathematical, Physical and Engineering Sciences*, 373(2033), 20140104. https://doi.org/10.1098/rsta.2014.0104.

Bozkus, Z., & Yildiz, O. (2004). Effects of inclination of bridge piers on scouring depth. *Journal of Hydraulic Engineering*, 130(8), 827–832. https://doi.org/10.1061/(asce)0733-9429(2004)130:8(827)

Chang, K., & Constantinescu, G. (2015). Numerical investigation of flow and turbulence structure through and around a circular array of rigid cylinders. *Journal of Fluid Mechanics*, 776, 161–199. https://doi.org/10.1017/jfm.2015.321

Chiatto, M., Shang, J. K., De Luca, L., & Grasso, F., (2021). Insights into low reynolds flow past finite curved cylinders. *Physics of Fluids*, 33(3). https://doi.org/10.1063/5.0043222.

Choi, S. U., & Choi, B. (2016). Prediction of time-dependent local scour around bridge piers. *Water and Environment Journal*, 30, n/a-n/a. https://doi.org/10.1111/wej.12157

Ettema, R., Melville, B. W., & Barkdoll, B. (1998). Scale effect in pier-scour experiments. *Journal of Hydraulic Engineering*, 124(6), 639–642. https://doi.org/10.1061/(ASCE)0733-9429(1998)124:6(639)

Euler, T., Zemke, J., Rodrigues, S., & Herget, J. (2014). Influence of inclination and permeability of solitary woody riparian plants on local hydraulic and sedimentary processes. *Hydrological Processes*, 28(3), 1358–1371. https://doi.org/10.1002/hyp.9655

Flowscience (2019). *Flow-3D User Manual*.

Graf, W. H. & Istiarto, I. (2002) Flow pattern in the scour hole around a cylinder, Journal of Hydraulic Research, 40(1), 13-20, http://doi.org/10.1080/00221680209499869.

Istiarto, I. (2001). *Flow Around a Cylinder in a Scoured Channel Bed*. Gadjah Mada University.

Jiang, F., Pettersen, B., Andersson, H. I., Kim, J., & Kim, S. (2018). Wake behind a concave curved cylinder. *Physical Review Fluids*, 3(9), 94804. https://doi.org/10.1103/PhysRevFluids.3.094804.

Jiang, F., Pettersen, B., & Andersson, H. I. (2019). Turbulent wake behind a concave curved cylinder. *Journal of Fluid Mechanics*, 878, 663–99. https://doi.org/10.1017/jfm.2019.648.

Kazemi, A. (2017). *Hydrodynamics of mangrove root-type models* (Issue December). Florida Atlantic University.

Keshavarzi, A., Shrestha, C., Ranjbar Zahedani, M., Ball, J., & Khabbaz, H. (2017). Experimental study of flow structure around two in-line bridge piers. *Proceedings of the Institution of Civil Engineers - Water Management*, 171, 1–17. https://doi.org/10.1680/jwama.16.00104

Kitsikoudis, V., Kirca, V. S. O., Yagci, O., & Celik, M. F. (2017). Clear water scour and flow field alteration around an inclined pile. *Coastal Engineering*, 129, 59–73. https://doi.org/10.1016/j.coastaleng.2017.09.001

Larsen, B. E., Fuhrman, D. R., & Sumer, B. M. (2016). Simulation of wave-plus-current scour beneath submarine pipelines. *Journal of Waterway, Port, Coastal, and Ocean Engineering*, 142(5), 04016003. https://doi.org/10.1061/(ASCE)WW.1943-5460.0000338

Majd, F. S., Yagci, O., Kirca, V. S. O., Kitsikoudis, V., & Lentsiou, E. N. (2016). *Flow and turbulence around an inclined pile*. Twenty-Sixth (2016) International Ocean and Polar Engineering Conference.

Minor, M., Zimmer, M., Helfer, V., Gillis, L., & Huhn, K. (2021). *Flow and sediment dynamics around structures in mangrove ecosystems—a modeling perspective* (pp. 83–120). https://doi.org/10.1016/B978-0-12-816437-2.00012-4

Moffatt, H. K. (1969). The degree of knottedness of tangled vortex lines. *Journal of Fluid Mechanics*, 35(1), 117–129. https://doi.org/10.1017/S0022112069000991

Moffatt, H. K., & Tsinober, A. (1992). Helicity in laminar and turbulent flow. *Annual Review of Fluid Mechanics*, 24(1), 281–312. https://doi.org/10.1146/annurev.fl.24.010192.001433

Moreau, J. J. (1961). Constantes d'un îlot tourbillonnaire en fluide parfait barotrope. *Comptes Rendus Hebdomadaires Des Séances de l'Académie Des Sciences*, 252(19), 2810.

Munson, B. R., Okiishi, T. H., Young, D. F. (2002) *Fundamentals of Fluid Mechanics*. 4th Edition, R. R. Donnelley & Sons, Chicago.

Nieuwstadt, F. T. M., Westerweel, J., & Boersma, B. J.

(2016). *Turbulence*. Springer International Publishing. https://doi.org/10.1007/978-3-319-31599-7

Norberg, C. (1994). An experimental investigation of the flow around a circular cylinder: Influence of aspect ratio. *Journal of Fluid Mechanics*, 258(April), 287–316. https://doi.org/10.1017/S0022112094003332

Rajani, B.N., Kandasamy, A., & Majumdar, S. (2012). On the reliability of eddy viscosity based turbulence models in predicting turbulent flow past a circular cylinder using URANS approach. *Journal of Applied Fluid Mechanics*, 5. http://doi.org/10.36884/jafm.5.01.11959.

Rosa, R. M. S. (2006). *Turbulence Theories*. Academic Press. https://doi.org/https://doi.org/10.1016/B0-12-512666-2/00111-5

Roulund, A., Sumer, B. M., Fredsøe, J., & Michelsen, J. (2005a). Numerical and experimental investigation of flow and scour around a circular pile. *Journal of Fluid Mechanics*, 534, 351–401. https://doi.org/10.1017/S0022112005004507

Roulund, A., Sumer, B. M., Fredsøe, J., & Michelsen, J. (2005b). Numerical and experimental investigation of flow and scour around a circular pile. *Journal of Fluid Mechanics*, 534, 351–401. https://doi.org/10.1017/S0022112005004507.

Shang, J. K., Stone, H. A., & Smits, A. J. (2018). Flow past finite cylinders of constant curvature. *Journal of Fluid Mechanics*, 837, 896–915. https://doi.org/10.1017/jfm.2017.884.

Sumer, B. M., & Fredsøe, J. (2006). *Hydrodynamics Around Cylindrical Structures.* Advanced Series on Ocean Engineering (Vol. 26). WORLD SCIENTIFIC. https://doi.org/10.1142/6248

Sumner, D. (2010). Two circular cylinders in crossflow: A review. *Journal of Fluids and Structures*, 26(6), 849–899. https://doi.org/10.1016/j.jfluidstructs.2010.07.001

Surry, J., & Surry, D. (1967). *The Effect of Inclination on the Strouhal Number and Other Wake Properties of Circular Cylinders at Subcritical Reynolds Numbers*. University of Toronto. Institute for Aerospace Studies.

Tesař, V. (2005). Time-mean helicity distribution in turbulent swirling jets. *Acta Polytechnica*, 45(6). https://doi.org/10.14311/776

Unger, J., & Hager, W. H. (2006). Down-flow and horseshoe vortex characteristics of sediment embedded bridge piers. *Experiments in Fluids*, 42(1), 1–19. https://doi.org/10.1007/s00348-006-0209-7

Wang, S., Yang, S., He, Z., Li, L., & Xia, Y. (2020). Effect of inclination angles on the local scour around a submerged cylinder. *Water* (Switzerland), 12(10), 1–20. https://doi.org/10.3390/w12102687

Yagci, O., Celik, M. F., Kitsikoudis, V., Ozgur Kirca, V. S., Hodoglu, C., Valyrakis, M., Duran, Z., & Kaya, S. (2016). Scour patterns around isolated vegetation elements. *Advances in Water Resources*, 97, 251–265. https://doi.org/10.1016/j.advwatres.2016.10.002

Yagci, O., Kirca, V. S. O., & Acanal, L. (2014). Wave attenuation and flow kinematics of an inclined thin plate acting as an alternative coastal protection structure. *Applied Ocean Research*, 48, 214–226. https://doi.org/10.1016/j.apor.2014.09.003

Yagci, O., Yildirim, I., Celik, M. F., Kitsikoudis, V., Duran, Z., & Kirca, V. S. O. (2017). Clear water scour around a finite array of cylinders. *Applied Ocean Research*, 68, 114–129. https://doi.org/10.1016/j.apor.2017.08.014

Yamamoto, K., & Hosokawa, I. (1981). A numerical study of inviscid helical turbulence. *Journal of the Physical Society of Japan*, 50(1), 343–348. https://doi.org/10.1143/JPSJ.50.343

Yu, X. (2002). Functional performance of a submerged and essentially horizontal plate for offshore wave control: A Review. *Coastal Engineering Journal*, 44(2), 127–147. https://doi.org/10.1142/S0578563402000470

Zimmerman, W. B. (1996). Fluctuations in passive tracers due to mixing by coherent structures in isotropic, homogeneous, helical turbulence. *IChemE Symposium Series*, 213–224.